USE OF IMPROVED WESTERGAARD STRESS FUNCTIONS TO ADEQUATELY SIMULATE THE STRESS FIELD AROUND CRACK TIPS

Elvis Yuri Mamani Vargas

Ney Augusto Dumont

elvismamani@hotmail.com

dumont@puc-rio.br

Civil Engineering Department

Pontifical Catholic University of Rio de Janeiro

Rua Marques de Sao Vicente, 225, 22451-900, Rio de Janeiro, Brazil

Abstract. *In the traditional boundary element methods, the numerical modeling of cracks is usually carried out by means of hypersingular fundamental solutions. A more natural procedure should make use of fundamental solutions (Green's functions) that represent the square-root singularity of the gradient field around the crack tip, which at most leads to improper integrals. Such a representation is best accomplished in a variationally-based framework that also addresses a convenient means of evaluating results at internal points. This is the subject of the present paper, with the use of generalized Westergaard stress functions for the numerical simulation of two-dimensional problems that may be completely unrelated to fracture mechanics. Problems of general topology can be modeled, such as in the case of unbounded and multiply-connected domains. The formulation is naturally applicable to notches and generally curved cracks. It also provides an easy means of approximating stress intensity factors. For a general-purpose code, Kelvin's and Westergaard-type fundamental solutions can be combined. It is shown that fundamental solutions corresponding to crack openings given by Hermitian polynomials lead to a better description of the stress field caused by a crack than as previously developed by the authors. A basic, validating numerical example is presented.*

Keywords: *Hybrid boundary elements, Fracture mechanics, Westergaard stress functions, Variational methods*

1 PREVIOUS DEVELOPMENTS AND MOTIVATION

1.1 Introduction

Tada *et al.* (1993, 1994) proposed a simple method for the construction of Westergaard-type stress functions for the analysis of fracture mechanics problems with either prescribed displacements or stresses. Their developments were restricted to the mathematical aspects of the formulation and to some analytical unfoldings. In the present paper the concept proposed by these authors is generalized and used for the construction of fundamental solutions in the hybrid boundary element method, which can be advantageously applied to classical elasticity problems and specifically to fracture mechanics (Dumont & Lopes, 2003; Dumont & Mamani, 2011a, 2011b, 2013). This formulation is directly applicable to notches as well as to internal or external curved cracks and enables the adequate description of high stress gradients, and is thus a simple means of evaluating stress intensity factors. Moreover, it is possible to use such stress functions to obtain in the frame of an iterative procedure the plastic zone around a crack tip (Dumont & Mamani, 2013). The present paper is a further generalization of the developments proposed by Dumont & Mamani (2011) toward the implementation of more accurate stress functions, as also illustrated with a basic, academical example.

1.2 Previous developments

A superposition of cracks was proposed by Dumont & Lopes (2002) to simulate cracks of general shape, as illustrated in Fig. 1. In the illustrative discretization, the curved crack is approximated by five nodal parameters. These nodal parameters are related to tractions given by Westergaard complex stress functions, applied as a succession of straight crack elements along the curved crack.

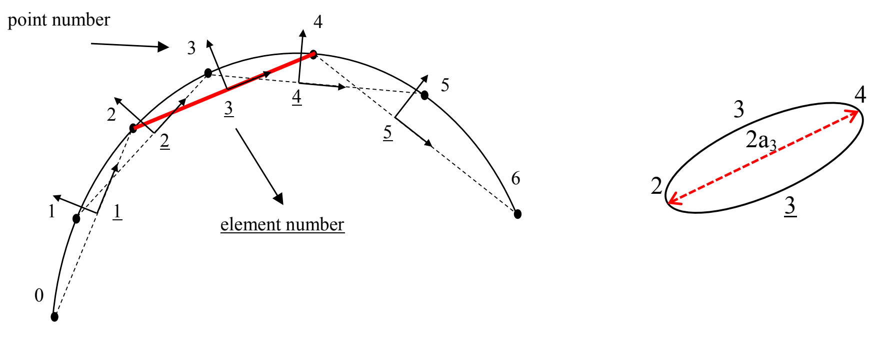

Figure 1: Illustration of the use of straight cracks to simulate generally curved cracks (Dumont and Lopes, 2003).

An improvement of these developments could be obtained later on by Dumont & Mamani (2011a, 2011b) in terms of superposed semicracks, as given by Eqs. (10) and (12) and illustrated in Fig. 2, not only to better fit curved cracks but also to simulate cavities, corners and notches. Based on these developments, Dumont & Mamani (2013) proposed the use of the model for the simulation of small plastic zones that develop and propagate around cracks (Fig. 3).

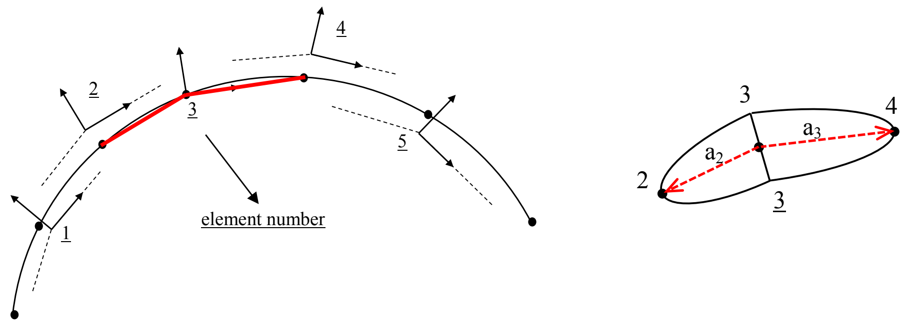

Figure 2: Illustration of the use of kinked cracks to simulate generally curved cracks (Dumont & Mamani, 2011).

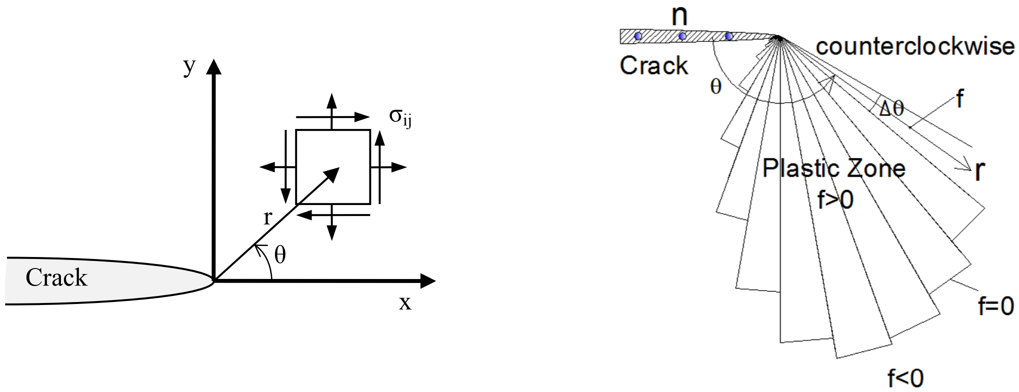

Figure 3: Local coordinate system, and partial construction of the plastic zone around a crack tip (Dumont & Mamani, 2013).

1.3 Motivation

The primary motivation to the present theoretical developments is a better simulation of the stress field around crack tips that may lead to accurate stress intensity factors as well as to the adequate representation of plastic zones. The elliptic semicrack proposed by Dumont & Mamani (2011a, 2011b, 2013), which seems efficient for the description of the stress field around crack tips, must be combined with crack elements of different shapes, so that spurious stress singularities can be avoided or minimized. The present proposition is the use of semielliptic cracks to represent crack tips only, with polynomial-shaped openings for the simulation of the rest of a crack face, as shown in Fig. (4).

2 BRIEF OUTLINE OF THE HYBRID BOUNDARY ELEMENT METHOD

The hybrid boundary element method (HBEM) was introduced in 1987 on the basis of the Hellinger-Reissner potential and as a generalization of Pian's hybrid finite element method (Pian, 1964; Dumont, 1989). The formulation requires evaluation of integrals only along the boundary and makes use of fundamental solutions (Green's functions) to interpolate fields in the domain. Accordingly, an elastic body of arbitrary shape may be treated as a single finite

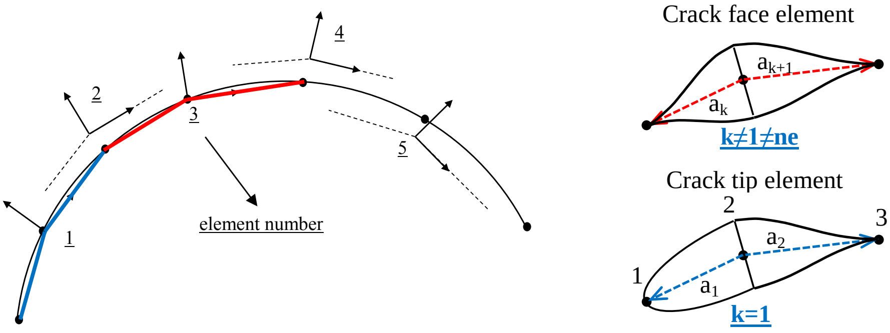

Figure 4: Illustration of the use of kinked cracks to simulate generally curved cracks (Mamani, 2015).

macro-element with as many boundary degrees of freedom as desired. In the meantime, the formulation has evolved to several application possibilities, including time-dependent problems (Dumont & Oliveira, 2001), fracture mechanics (Dumont & Lopes, 2003), non-homogeneous materials (Dumont *et al.*, 2004) and strain gradient elasticity (Dumont & Huamán, 2009)).

The brief outline of Sections 2.1-2.3 is presented according to Dumont & Mamani (2011).

2.1 Problem Formulation

An elastic body is submitted to body forces b_i in the domain, tractions $\bar{t}_i$ on part Γ_σ of the boundary Γ and to displacements $\bar{u}_i$ on the complementary part Γ_u. The task is to find the best approximation for stresses and displacements, σ_{ij} and u_i, such that

$$\sigma_{ji,j} = b_i \quad \text{in the domain} \quad \Omega, \tag{1}$$
$$u_i = \bar{u}_i \quad \text{along} \quad \Gamma_u \quad \text{and} \quad t_i = \sigma_{ij}\, n_j = \bar{t}_i \quad \text{along} \quad \Gamma_\sigma \tag{2}$$

in which n_j is the outward unit normal to the boundary. Indicial notation is used.

2.2 Stress and Displacement Assumptions

Two independent trial fields are assumed (Pian,1964; Dumont, 1989). The displacement field is explicitly approximated along the boundary by u_i^d, where $(\,)^d$ means *displacement assumption*, in terms of polynomial functions u_{im} with compact support and nodal displacement parameters $\mathbf{d} = [d_m] \in \mathbb{R}^{n^d}$, for n^d displacement degrees of freedom of the discretized model. An independent stress field σ_{ij}^s, where $(\,)^s$ stands for *stress assumption*, is given in the domain in terms of a series of fundamental solutions $\sigma_{ij\,m}^*$ with global support, multiplied by force parameters $\mathbf{p}^* = [p_m^*] \in \mathbb{R}^{n^*}$ applied at the same boundary nodal points m to which the nodal displacements d_m are attached ($n^* = n^d$), plus some particular solution σ_{ij}^p due to body forces, for instance. Displacements u_i^s are obtained from σ_{ij}^s. Then,

$$u_i^d = u_{im}\, d_m \quad \text{on} \quad \Gamma \quad \text{such that} \quad u_i^d = \bar{u}_i \quad \text{on} \quad \Gamma_u \quad \text{and} \tag{3}$$
$$\sigma_{ij}^s = \sigma_{ijm}^*\, p_m^* + \sigma_{ij}^p \quad \text{such that} \quad \sigma_{jim,j}^* = 0 \quad \text{in} \quad \Omega \tag{4}$$
$$\Rightarrow \quad u_i^s = u_{im}^*\, p_m^* + u_{is}^r\, C_{sm}\, p_m^* + u_i^p \quad \text{in} \quad \Omega \tag{5}$$

where u_{im}^* are displacement fundamental solutions corresponding to σ_{ijm}^*. Rigid body motion is included in terms of functions u_{is}^r multiplied by in principle arbitrary constants C_{sm} (Dumont, 1989).

2.3 Governing Matrix Equations

The Hellinger-Reissner potential, as implemented by Pian (1964) on the basis of the two-field assumptions of the latter Section and generalized by Dumont (1989), leads to two matrix equations that express nodal equilibrium and compatibility requirements:

$$\mathbf{H}^{\mathrm{T}}\,\mathbf{p}^* \quad = \quad \mathbf{p}-\mathbf{p}^p \tag{6}$$

$$\mathbf{F}^*\mathbf{p}^* \quad = \quad \mathbf{H}(\mathbf{d}-\mathbf{d}^p) \tag{7}$$

in which $\mathbf{H} = [H_{nm}] \in \mathbb{R}^{n^d\times n^*}$ is the same double-layer potential matrix of the collocation boundary element method (Brebbia *et al.*, 1984), and $\mathbf{p} = [p_n] \in \mathbb{R}^{n^d}$ are equivalent nodal forces obtained as in the finite element method. Moreover, $\mathbf{F}^* = [F^*_{nm}] \in \mathbb{R}^{n^*\times n^*}$ is a symmetric, flexibility matrix. The matrices $\mathbf{H}$ and $\mathbf{F}^*$ may be compactly defined as

$$[H_{mn} \quad F^*_{mn}] = \int_\Gamma \sigma^*_{ijm} n_j \left\langle u_{in} \quad u^*_{in}\right\rangle \mathrm{d}\Gamma \tag{8}$$

Solving for $\mathbf{p}^*$ in Eq. (6), one arrives at the matrix system

$$\mathbf{H}^{\mathrm{T}}\mathbf{F}^{*(-1)}\mathbf{H}(\mathbf{d}-\mathbf{d}^p) = \mathbf{p}-\mathbf{p}^p \tag{9}$$

where $\mathbf{H}^{\mathrm{T}}\mathbf{F}^{*(-1)}\mathbf{H} \equiv \mathbf{K}$ is a stiffness matrix. The inverse $\mathbf{F}^{*(-1)}$ must be evaluated in terms of generalized inverses, as $\mathbf{F}^*$ is singular for a finite domain Ω (Dumont, 1989, 2016). Results at internal points are expressed in terms of Eqs. (4) and (5) after evaluation of $\mathbf{p}^*$.

Since evaluating $\mathbf{F}$ and solving for $\mathbf{p}^*$ in Eq. (7) is very time consuming, a simplified hybrid boundary formulation has been developed (Dumont & Aguilar, 2011) to completely circumvent the matrix operations described in the latter paragraph. On the other hand, the present problem of fracture mechanics is usually formulated for Neumann-type boundary conditions, for which Eq. (6) is sufficient and only the evaluation of the double-layer potential matrix $\mathbf{H}$ is required.

3 STRESS FUNCTIONS

Fundamental solutions (Green's functions) may be obtained for a semicrack of length a_1 along a straight line that is rotated in the counter clock direction by an angle θ_1, as illustrated in Fig. 5, with which it is possible to compose kinked cracks of any length (Dumont, 2008) as illustrated in Fig. 7. Tada *et al.* (1993, 1994) propose the complex potential function

$$\Phi(z) = -\frac{1}{2\pi}\int_0^{a_1} \frac{f(x)}{Z_1 - x}\mathrm{d}x \tag{10}$$

for a crack of general shape $f(x)$ along the x axis. To make calculations as simple as possible, the shape function is initially defined for a semicrack (numbered as 1, indicated by the subscript) with length $a_1 = 1$ and the integration of Eq. (10) is carried out in the interval [0, 1], generally applied to a crack rotated by an angle θ_1, such that

$$Z_1 = zT_1 \text{ with } \mathrm{T}_1 = \frac{1}{\mathrm{a}_1}(\cos\theta_1 - \mathrm{i}\sin\theta_1) \tag{11}$$

As explored in the present framework (Dumont, 2008; Mamani, 2015), the following crack opening expressions are given:

$$f(x)=\sqrt{1-x^2} \quad \text{for an elliptic semicrack opening} \tag{12}$$

$$f(x)=2x^3-3x^2+1 \quad \text{for a polynomial semicrack opening} \tag{13}$$

$$f(x)=x\sqrt{1-x^2} \quad \text{for an elliptic semicrack rotation} \tag{14}$$

$$f(x)=x^3-2x^2+x \quad \text{for a polynomial semicrack rotation} \tag{15}$$

Observe that Eqs. (13) and (15) are Hermitian polynomials for $x \in (0,1)$, as used to simulate beam elements, corresponding respectively to unit displacement and unit drilling rotation at $x=0$. The crack openings corresponding to these functions are illustrated in Fig. 5. Although not strictly required, all four functions introduced above are also used as shape functions u_{im} to express u_i^d in Eq. (3), as used in the definition of $\mathbf{H}$ in Eq. (8).

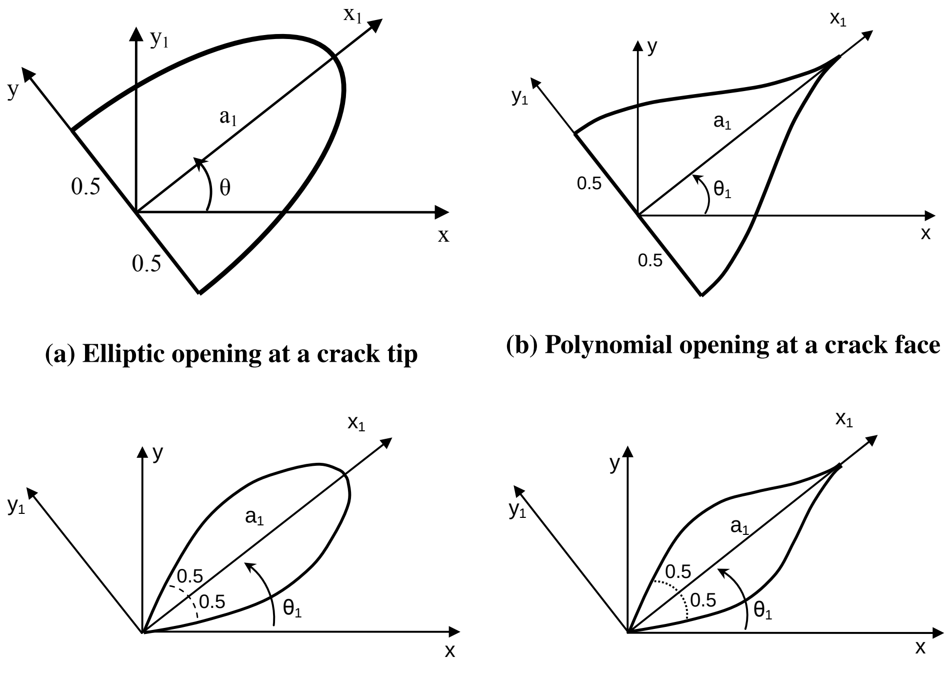

(a) Elliptic opening at a crack tip **(b) Polynomial opening at a crack face**

(c) Rotation adjacent to a crack tip **(d) Rotation at a crack face**

Figure 5: Semicracks of length a_1 rotated by an angle θ_1 (Dumont & Mamani, 2015).

The expression of Eq. (10) and its derivatives for the semicrack of the Eq. (12) are (elliptic opening at the crack tip)

$$\Phi_1 = \frac{\sqrt{1-Z_1^2}}{2\pi} \ln\left(\frac{-1-\sqrt{1-Z_1^2}}{Z_1}\right) - \frac{2+Z_1\pi}{4\pi} \tag{16}$$

$$\Phi_1' = -\frac{Z_1}{2\pi\sqrt{1-Z_1^2}} \ln\left(\frac{-1-\sqrt{1-Z_1^2}}{Z_1}\right) - \frac{2+\pi Z_1}{4\pi Z_1} \tag{17}$$

$$\Phi_1'' = -\frac{1}{2\pi\left(1-Z_1^2\right)^{3/2}} \ln\left(\frac{-1-\sqrt{1-Z_1^2}}{Z_1}\right) + \frac{1}{2\pi Z_1^2\left(1-Z_1^2\right)} \tag{18}$$

The expression of Eq. (10) and its derivatives for the semicrack of the Eq. (13) are (polynomial opening at the crack face)

$$\Phi_1 = \frac{1-3Z_1^2+2Z_1^3}{2\pi}\ln\left(\frac{Z_1-1}{Z_1}\right) - \frac{1}{12\pi}\left(5+12Z_1-12Z_1^2\right) \tag{19}$$

$$\Phi_1' = -\frac{3Z_1\left(1-Z_1\right)}{\pi}\ln\left(\frac{Z_1-1}{Z_1}\right) - \frac{1}{2\pi}\left(\frac{1}{Z_1}+3-6Z_1\right) \tag{20}$$

$$\Phi_1'' = -\frac{3\left(1-2Z_1\right)}{\pi}\ln\left(\frac{Z_1-1}{Z_1}\right) + \frac{1}{2\pi Z_1^2}\left(1+12Z_1^2\right) \tag{21}$$

The expression of Eq. (10) and its derivatives for the semicrack of the Eq. (14) are (drilling rotation adjacent to the crack tip)

$$\Phi_1 = \frac{Z_1\sqrt{1-Z_1^2}}{2\pi}\ln\left(\frac{-1-\sqrt{1-Z_1^2}}{Z_1}\right) - \frac{-\pi+4Z_1+2\pi Z_1^2}{8\pi} \tag{22}$$

$$\Phi_1' = -\frac{2Z_1^2-1}{2\pi\sqrt{1-Z_1^2}}\ln\left(\frac{-1-\sqrt{1-Z_1^2}}{Z_1}\right) - \frac{2+\pi Z_1}{2\pi} \tag{23}$$

$$\Phi_1'' = -\frac{2Z_1^3-3Z_1}{2\pi\left(1-Z_1^2\right)^{3/2}}\ln\left(\frac{-1-\sqrt{1-Z_1^2}}{Z_1}\right) + \frac{-1-\pi Z_1+2Z_1^2+\pi Z_1^3}{2\pi Z_1\left(1-Z_1^2\right)} \tag{24}$$

Finally, for the expression of Eq. (10) and its derivatives applied to the semicrack of the Eq. (15) are (drilling rotation at the crack face)

$$\Phi_1 = \frac{Z_1-2Z_1^2+Z_1^3}{2\pi}\ln\left(\frac{Z_1-1}{Z_1}\right) - \frac{1}{12\pi}\left(-2+9Z_1-6Z_1^2\right) \tag{25}$$

$$\Phi_1' = \frac{1-4Z_1+3Z_1^2}{2\pi}\ln\left(\frac{Z_1-1}{Z_1}\right) - \frac{1}{4\pi}\left(5-6Z_1\right) \tag{26}$$

$$\Phi_1'' = \frac{-2+3Z_1}{\pi}\ln\left(\frac{Z_1-1}{Z_1}\right) - \frac{1}{2\pi Z_1}\left(1+6Z_1\right) \tag{27}$$

4 THE CRACK MODELING PROBLEM

4.1 Basic developments

Independently from the proposed stress function, as shown in the previous section, the mode I and mode II crack opening displacement and stress expressions for plane strain are (Mamani, 2011; Dumont & Mamani, 2011)

$$\mathbf{u}^I_{1(0)} = \frac{1+\nu}{E}\begin{Bmatrix} (1-2\nu)\mathrm{Re}\Phi_1 - \dfrac{y_1}{a_1}\mathrm{Im}\Phi_1' \\ 2(1-\nu)\mathrm{Im}\Phi_1 - \dfrac{y_1}{a_1}\mathrm{Re}\Phi_1' \end{Bmatrix}, \quad \sigma^I_{1(0)} = \begin{bmatrix} \dfrac{1}{a_1}\mathrm{Re}\Phi_1' - \dfrac{y_1}{a_1^2}\mathrm{Im}\Phi_1'' \\ \dfrac{1}{a_1}\mathrm{Re}\Phi_1' + \dfrac{y_1}{a_1^2}\mathrm{Im}\Phi_1'' \\ -\dfrac{y_1}{a_1^2}\mathrm{Re}\Phi_1'' \end{bmatrix} \tag{28}$$

$$\mathbf{u}^{II}_{1(0)} = \frac{1+\nu}{E}\left\{\begin{array}{c} 2(1-\nu)\mathrm{Im}\Phi_1 + \dfrac{y_1}{a_1}\mathrm{Re}\Phi_1' \\ -(1-2\nu)\mathrm{Re}\Phi_1 - \dfrac{y_1}{a_1}\mathrm{Im}\Phi_1' \end{array}\right\}, \quad \sigma^{II}_{1(0)} = \begin{bmatrix} \dfrac{2}{a_1}\mathrm{Im}\Phi_1' + \dfrac{y_1}{a_1^2}\mathrm{Re}\Phi_1'' \\ -\dfrac{y_1}{a_1^2}\mathrm{Re}\Phi_1'' \\ \dfrac{1}{a_1}\mathrm{Re}\Phi_1' - \dfrac{y_1}{a_1^2}\mathrm{Im}\Phi_1'' \end{bmatrix} \tag{29}$$

The subscript $()_{(0)}$ in the above equations means that all quantities are referred to the local Cartesian system (x_1, y_1) and must be consequently rotated to the global system.

A general kinked crack is obtained by combining two semicracks, as illustrated in Fig. 6 for two elliptic semicracks. All mathematical developments including consistency and continuity checks are given by Dumont & Mamani (2011). The $1/\sqrt{r}$ behavior of stresses, for $r \to 0$ at the crack tips, is observed independently from size and orientation of the semicracks. Although there is no singularity at the interface of the semicracks, a $\ln(\xi)$ term (for $\xi \to 0$) indicates that a special numerical integration scheme must be used in the vicinity of such interfaces when either $a_1 \neq a_2$ or $\theta_2 - \theta_1 \neq \pi$ (Dumont & Mamani, 2011; Mamani, 2015).

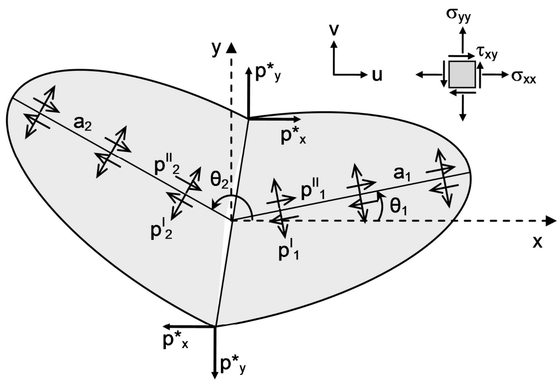

Figure 6: General kinked crack as an assemblage of two elliptic semicracks.

Figure 7 shows the combinations of two semicracks for the crack opening expressions given in Eqs. (12-15) and illustrated in Fig. 6. Observe that two rotating crack shapes lead to a partial overlap of the crack faces, which is mechanically not feasible. However, this does not occur in practice as a rotation is always superposed with an opening.

In the following developments, a combination of two elliptic semicracks, as illustrated in Fig. 6, will be called an *elliptic element*; the use of an elliptic semicrack and a polynomial semicrack to model the crack tip [shown as (b) in Fig. 7] together with two polynomial semicracks for the crack face [shown as (a) in the figure] will be referred to as a *mixed element*; and the latter case with the additional rotating possibility, as shown in the lower row of Fig. 7 for a segment either inside the crack (c) or at the crack tip (d) will correspond to a *mixed element with rotation* and will require an additional degree of freedom to be described. The illustrations of Figs. 5 and 7 can be easily visualized for a mode I crack opening, but are less intuitive in the case of Fig. 6, for example, when there is a contribution of the mode II stress state. In fact, the illustrations of Figs. 5 and 7 are equally valid for the mode II stress configuration, as already inferred from Eqs. 28 and 29 and comprehensively laid down by Dumont and Mamani (2011) for the elliptic element.

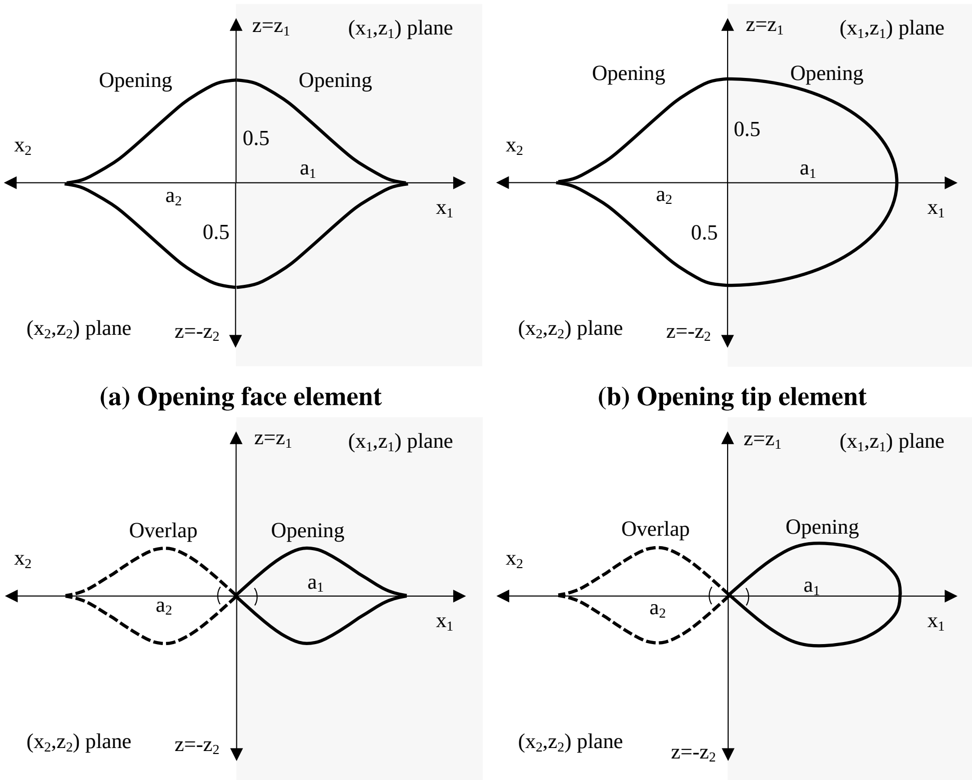

(a) Opening face element **(b) Opening tip element**

(c) Rotating face element **(d) Rotating tip element**

Figure 7: Elements used to discretize a crack in terms of openings and drilling rotations.

4.2 Numerical evaluation of the crack opening

The simplest case of a horizontal crack in a continuous, isotropic and infinite medium and submitted to a mode I stress field, as illustrated on the left in Fig. 8, is investigated in order to numerically assess the formulation proposed in the previous section. In fact, it is the authors' experience that the numerical issues related to any complicated cracked configuration (including multiple and curved cracks) and any domain topology can be brought down to the stress description issues around a single, straight crack's tip (Dumont & Lopes, 2003; Dumont & Mamani, 2011). The crack under investigation has a length $2a = 2.0$ and the material properties are such that $E/(1-\nu^2) = 2$. Thus, the target, analytical solution of this problem corresponds to an elliptic opening of unit value, as indicated on the upper left in Fig. 9. The crack is modeled with combinations of elliptic and polynomial semicracks, as illustrated on the right in Fig. 8 for a discretization with five elements. All input and output quantities are given in consistent unities. When not otherwise indicated, all assessments are in terms of the hybrid boundary element method.

The results for simulations with 16 nodes in terms of either elliptic elements, mixed elements or mixed elements with drilling rotation is shown in Fig. 9. Since this is a mode I problem, the former two cases actually require only one degree of freedom per element, while in the latter case there is a total of 32 degrees of freedom. The numerical results are evaluated using Eq. (6) to solve for $\mathbf{p}^*$ and then Eq. (5) to directly express the opening displacements along the crack face, as given on the upper left in Fig. 9. The error differences can be better

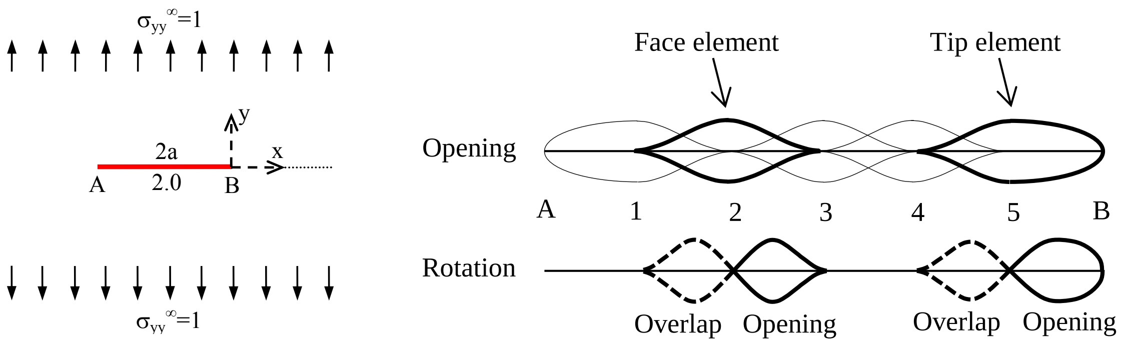

Figure 8: Straight crack in the open domain submitted to a remote uni-axial stress field (left), and modeling with crack elements using five nodes (right).

visualized in the graph below in the figure using as error norm

$$\epsilon\,(\%) = \left| \frac{u_{num} - u_{ana}}{u_{ana(max)}} \right| \times 100\% \tag{30}$$

where, in the case, $u_{ana(max)} = 1$. The results with mixed elements are a significant improvement in comparison with the case of plain elliptic elements (both analyses with 16 degrees of freedom). The best results are by far the ones using mixed elements with rotation, although one should bear in mind that they correspond to the double amount of degrees of freedom. The graph on the upper right in Fig. 9 is a zoom of the results on the left for $x \in (0.7, 1)$, to show that the added rotational degrees of freedom significantly contribute to smoothen the displacements and then arrive at more accurate results.

Figure 10 shows a convergence study for the problem of Fig. 8 using 4, 16 and 64 mixed elements with drilling rotation, as implemented in the hybrid boundary element method. The crack opening results are visually of excellent quality already for the case with four elements. The error analysis on the right shows that the convergence is not everywhere monotonic, although this is observed globally.

Assessment in terms of the conventional boundary element method. The conventional boundary element method is also tested in this section. The fundamental solutions (Green's functions) proposed in Section 3 are used in the matrix system

$$\mathbf{Hd} = \mathbf{Gt} + \mathbf{b} \tag{31}$$

where $\mathbf{H}$ is the same double-layer potential matrix defined in Eq. (8), exactly as for the hybrid boundary element method, and $\mathbf{G}$ is the single-layer potential matrix, which uses the same functions of Eqs. (12-15) to interpolate the traction forces [as implemented by Mamani (2015), although not strictly required]. Since the body-force term $\mathbf{b}$ in the above equation refers to a constant stress state, it can be easily brought down to the crack boundary.

Figure 11 shows the same kind of results of Fig. 9 for opening boundary displacements interpolated from the evaluated nodal data $\mathbf{d}$. At least in this case, the results with the conventional boundary element method are not as accurate as in the hybrid formulation. However, convergence is everywhere monotonic, as observed in the opening-error graph on the right.

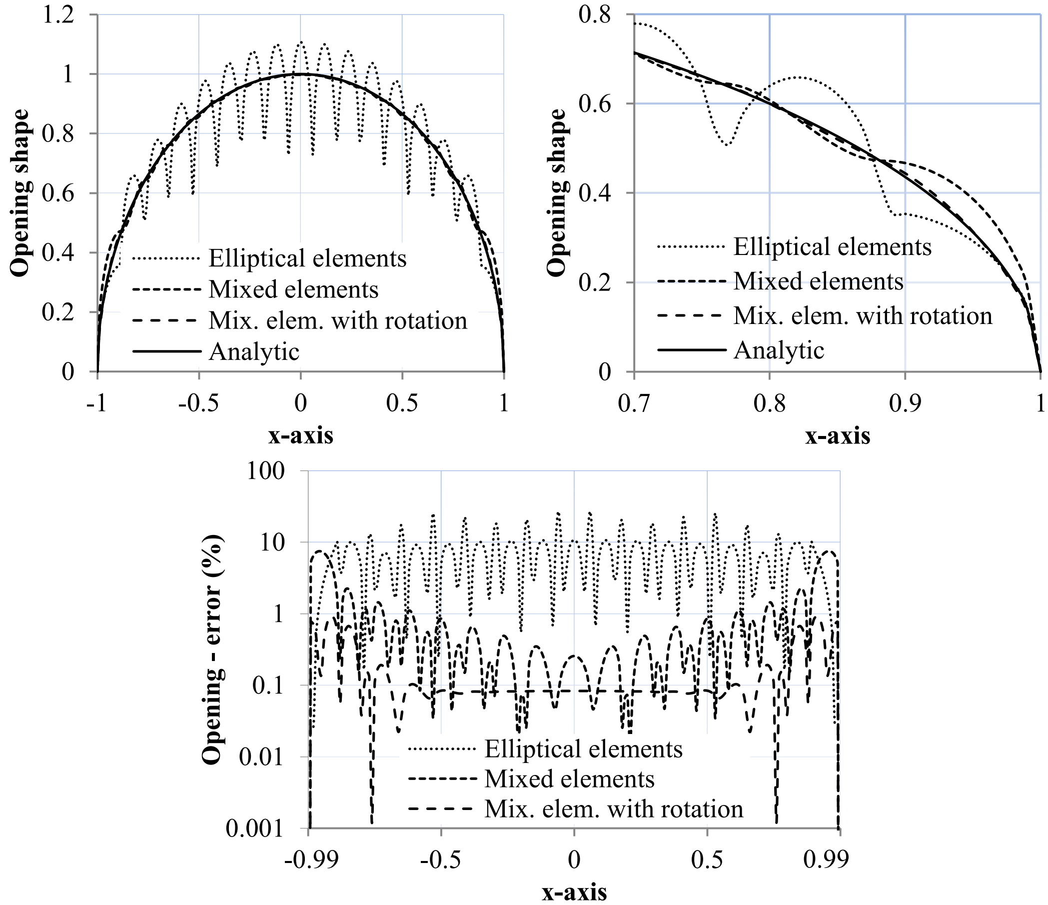

Figure 9: Opening displacements ((upper left and zoom on the right)) and corresponding errors (below) for the straight crack of Fig. 8 discretized with 16 **elements in an analysis with the hybrid boundary element method.**

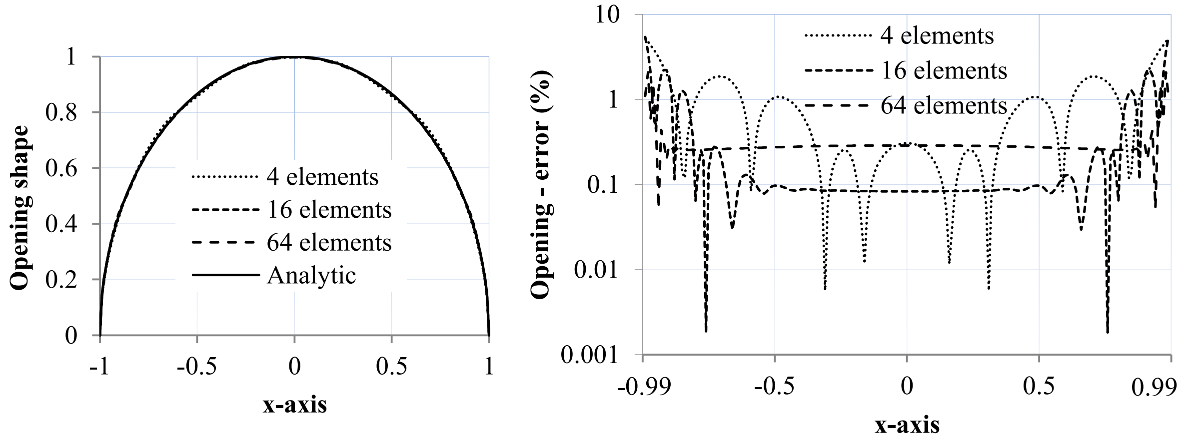

Figure 10: Opening displacements (left) and corresponding errors (right) for the straight crack of Fig. 8 using mixed elements with rotation in an analysis with the hybrid boundary element method.

4.3 An assessment of the stress field around the crack tip

The same problem on the left in Fig. 8 is used to assess the stress field around a crack tip. The normal stress σ_{yy} is plotted on the left in Fig. 12 along the line segment $(x = 0..1, y =$

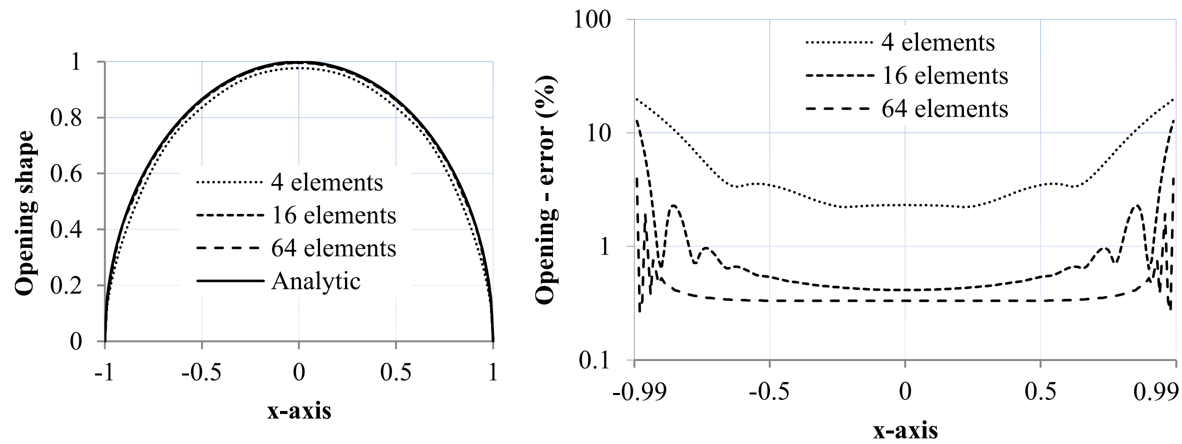

Figure 11: Opening displacements (left) and corresponding errors (right) for the straight crack of Fig. 8 using mixed elements with rotation in the conventional boundary element method.

0), according to the Cartesian system shown in Fig. 8, for the crack modeled with several different numbers of elliptic elements. The results are visually almost indistinguishable from the analytic ones. However, an analysis along the line segment $(x = 0.0001..100, y = 0)$ shows a pronounced oscillation of the errors in the near field, even though they tend to zero for points far from the crack tip. This oscillation prevents the use of a reliable method to arrive at an accurate stress intensity factor.

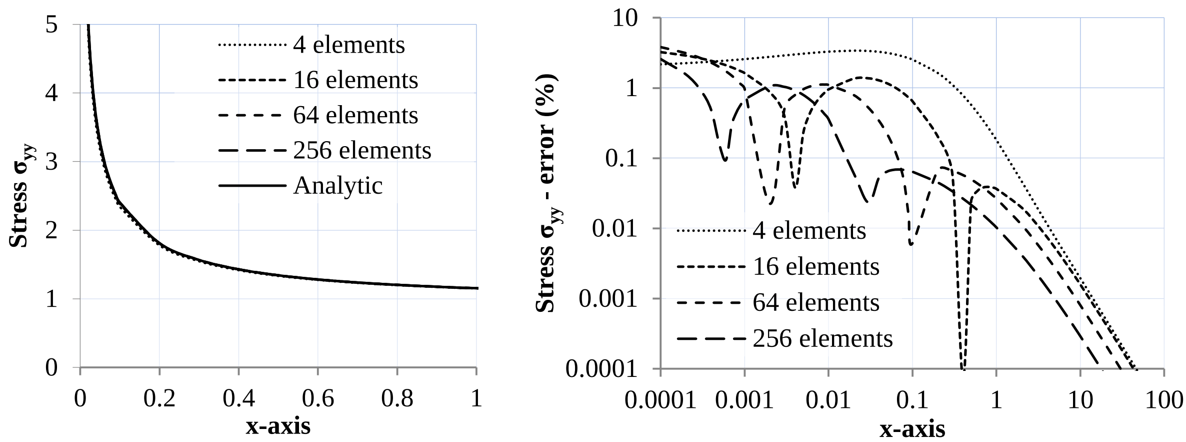

Figure 12: Stress σ_{yy} values (left) and error (right) in points along the dashed line on the left of Fig. 8 using elliptic elements.

The same analysis is carried out for mixed elements and it is not possible to recognize an improvement in the stress field, as compared with results of the previous figure.

Finally, Fig. 14 shows similar results as in the previous two figures, but this time for simulations with mixed elements including drilling rotation. The results improve significantly both in terms of accuracy and by presenting no oscillations as one takes into account points increasingly far from the crack tip. Then, one is entitled to conclude that this discretization model shall lead to more robust and reliable schemes for the evaluation of stress intensity factors as well as in the estimate of the plastic zone around a crack tip.

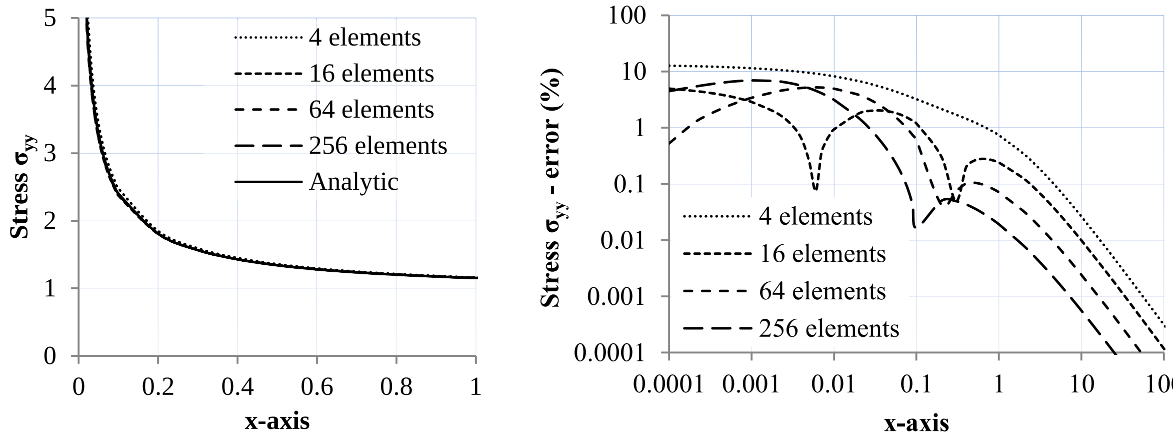

Figure 13: Stress σ_{yy} values (left) and corresponding error diagrams (right) at points along the dash line on the left of Fig. 8 using mixed elements (rotation not included).

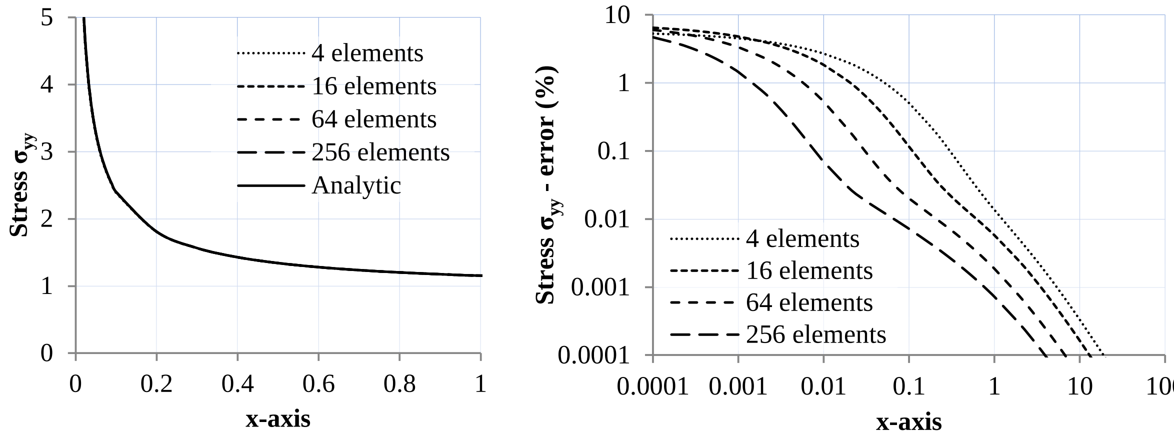

Figure 14: Stress σ_{yy} values (left) and corresponding error diagrams (right) at points along the dash line on the left of Fig. 8 using mixed elements with drilling rotation.

4.4 Stress intensity factor evaluated from the force parameters $\mathbf{p}^*$

After solving Eq. (6) for the force parameters $\mathbf{p}^*$, the most immediate means of arriving at a stress intensity factor estimate is from its definition

$$K_I = \lim_{r \to 0} \sqrt{2\pi r}\sigma_{yy}(r,\theta) \tag{32}$$

for σ_{yy} obtained from the terms of $\mathbf{p}^*$ referred to the crack tip. For the mode I problem of Fig. 8 [see Mamani (2015) for the general mode I and mode II expression], one obtains

$$K_{I(n)} = \frac{\sqrt{\pi a_n}}{2a_n}\left(p^*_{y(n)} + \frac{1}{3}p^*_{ry(n)}\right) \tag{33}$$

where a_n is the semicrack length at the crack tip (it would be a_1 on the right in Fig. 7) and $p^*_{y(n)}$ and $p^*_{ry(n)}$ are the force parameters corresponding to the opening shapes – displacement and drilling rotation – on the right of the same Fig. 7. The results for 1, 4, 16, 64 and 256 elements is given on the left in Fig. 15. Although the results have been shown to converge for stresses in the vicinity of the crack tip, as in the previous figures, absolute convergence cannot be observed in this case – and cannot be demonstrated by any theorem, since this is a localized behavior (how the stress goes locally to infinity) for which no energy norm can be given (Dumont & Lopes, 2003). It is even surprising that the results for elliptic elements do converge better than in the case of the generally more accurate implementation with mixed elements with drilling rotation (6% accuracy agains 8%). Also, observe that, in the present case, the result for just one crack element trivially coincides with the analytic solution.

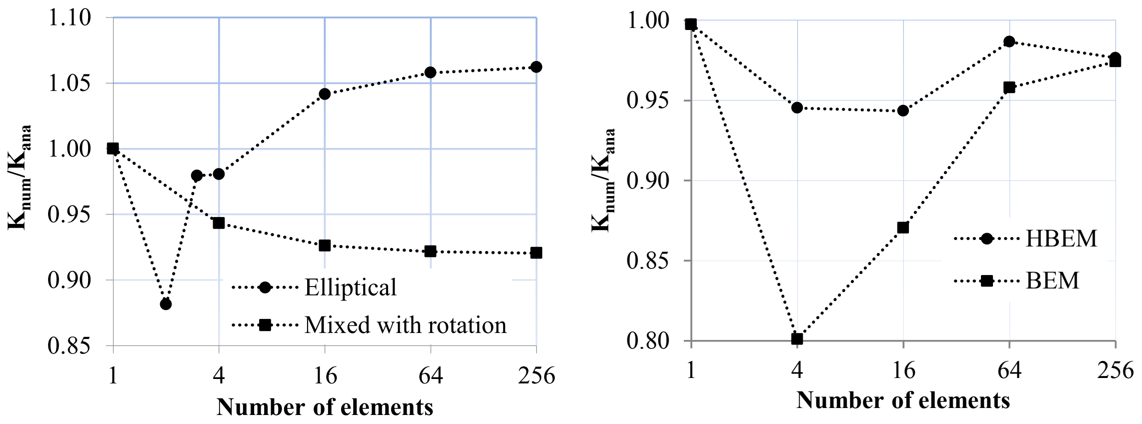

Figure 15: Stress intensity factors for the straight crack of Fig. 8 obtained (left) from Eq. (33) **for elliptic and mixed elements with rotation, and (right) in terms of the crack tip opening displacement.**

4.5 Stress intensity factor evaluated from the crack tip opening

The stress intensity factor may be obtained from the crack tip opening displacement:

$$K_I = \frac{2G}{\kappa + 1} \lim_{r \to 0} \sqrt{\frac{2\pi}{r}} u_y(r, \pi) \tag{34}$$

where $\kappa = 3 - 4\nu$ for plane strain and $\kappa = (3 - \nu)/(1 + \nu)$ for plane stress. Such results are usually more accurate than in terms of the stress field, as shown on the right in Fig. 15 for u_y evaluated at a distance of 0.01 from the crack tip using the hybrid as well as the conventional boundary element methods. Although no convergence can be demonstrated also in this case, the results (errors about 3%) are better than the ones reported by Anderson (1995) for a finite element mesh with 2000 nodes (errors about 5%).

4.6 Stress intensity factor evaluated from stresses

For the crack of Fig. 8, a simple and direct estimate of the stress intensity factor is by using Eq. (32), where in practice r is given a very small value, also with $\theta = 0$. The analytical solution for the crack problem of Fig. 8 is $K_I = \sqrt{\pi}$. The graph on the left in Fig. 16 shows the relation between numerically evaluated stress intensity factors for $r = 0.001$, 0.01 and 0.1, using Eq. (32), and the analytical, target one . Another possibility would be the extrapolation of the above values to obtain results at $r = 0$. However, there is an oscillation as $r \to 0$, which renders such a procedure not reliable.

An alternative to estimate the stress intensity factor is by comparison with the Williams' series, as explored, for instance, by Lopes (2002). As first shown by Williams (1957), the stress expression around a crack tip is, in polar coordinates,

$$\sigma_{rr} = \frac{1}{4\sqrt{r}}\left[s_1\left(-5\mathbf{cos}\frac{\theta}{2} + \mathbf{cos}\frac{3\theta}{2}\right) + t_1\left(-5\mathbf{sin}\frac{\theta}{2} + 3\mathbf{sin}\frac{3\theta}{2}\right)\right] + 4s_2\mathbf{cos}^2\theta... \quad (35)$$

$$\sigma_{\theta\theta} = \frac{1}{4\sqrt{r}}\left[s_1\left(-3\mathbf{cos}\frac{\theta}{2} - \mathbf{cos}\frac{3\theta}{2}\right) + t_1\left(-3\mathbf{sin}\frac{\theta}{2} - 3\mathbf{sin}\frac{3\theta}{2}\right)\right] + 4s_2\mathbf{sin}^2\theta... \quad (36)$$

$$\sigma_{r\theta} = \frac{1}{4\sqrt{r}}\left[s_1\left(-\mathbf{sin}\frac{\theta}{2} - \mathbf{sin}\frac{3\theta}{2}\right) + t_1\left(\mathbf{cos}\frac{\theta}{2} + 3\mathbf{cos}\frac{3\theta}{2}\right)\right] - 2s_2\mathbf{sin}2\theta... \quad (37)$$

The constants s_1 and t_1 are related to mode I and mode II stress intensity factors by

$$s_1 = -\frac{K_I}{\sqrt{2\pi}} \quad \text{and} \quad t_1 = \frac{K_{II}}{\sqrt{2\pi}} \quad (38)$$

Then, it is possible to evaluate σ_{yy} at a series of points departing from as close as possible to $r = 0$ along the x axis and fit using least squares the series given according to Eqs. (35-37).

The graph on the right in Fig. 16 displays the stress intensity factor results for five terms of the Williams' series (the first term is the one of actual interest) obtained from ten numerical values σ_{yy} for $r \in (0.001, 0.01)$, $r \in (0.01, 0.1)$ and $r \in (0.01, 0.1)$ along the x axis. Observe that the analytic solution is trivially obtained for one single crack element.

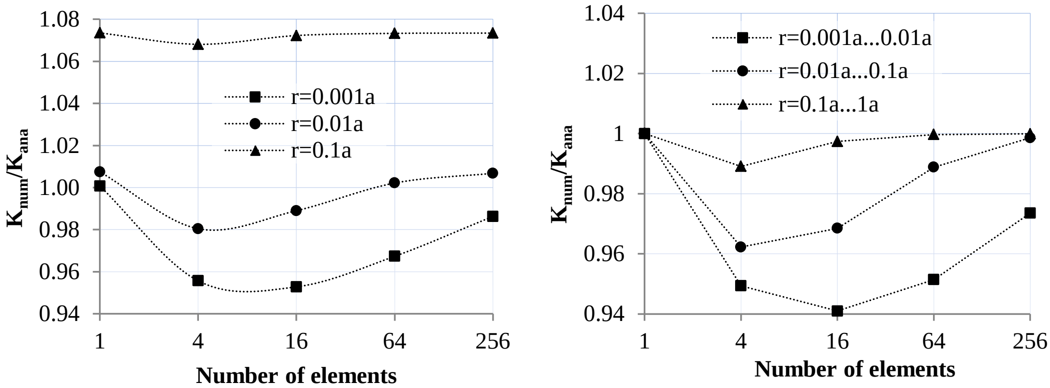

Figure 16: Stress intensity factors of the straight crack of the Fig. 8 obtained at several close points r (left) as well as in terms of the Williams' series (right).

CONCLUDING REMARKS

The implemented crack tip elements provide a simple and efficient means for the description of the stress field around crack tips. Although the combination of generalized Westergaard functions and Kelvin's fundamental solutions has shown to be efficient in terms of the global behavior of a cracked elastic body (Lopes, 1998, 2002; Dumont and Lopes, 2003; Dumont and Mamani, 2011, 2013; Mamani, 2011, 2015), some improvements have become mandatory from the preliminary investigations as regarding the very local phenomenon of stresses going to infinity. In fact, the elliptic semicracks, which seem efficient for the description of the stress field around crack tips, must be combined with crack elements of different shapes, so that spurious high stress gradients along the crack face can be avoided or minimized, as shown by means of several numerical assessments. The numerical examples of Section 4 have been analyzed for biaxial stress states, as well, with similar results as the ones displayed. The present developments for a single straight crack in the open domain lead to a better understanding of the more complex cases of multiply connected and multiply cracked, irregularly shaped domains under complicated load combinations. Evaluations of the stress intensity factor in terms of the J integral have already been carried out by Lopes (2002) and Mamani (2011) using only elliptic elements. Evaluations for the J integral using the proposed improved elements, not given in this paper, show improvements, which are however not significant. The general conclusion is that no monotonic convergence can be demonstrated for evaluations of stress intensity factors, since there seems to be no energy theorem related to this local phenomenon. A code for general applications is available and some results have already been published (Dumont and Lopes, 2003; Dumont and Mamani, 2011). The code for the simulation of plastic zones around crack tips, as developed by Dumont and Mamani (2013), is now being implemented with the more general shapes proposed in the present paper.

ACKNOWLEDGEMENTS

This project was supported by the Brazilian agencies CAPES, CNPq and FAPERJ.

REFERENCES

Anderson, T. L., 1995. *Fracture Mechanics: Fundamentals and Applications*. 2. ed. CRC Press. Boca Raton, New York.

Ang, W. T. & Telles, J. C. F., 2004. A numerical Green's function for multiple cracks in anisotropic bodies, *Journal of Engineering Mathematics*, vol. 49, issue 3, pp. 197-207.

Barenblatt, G. I., 1962. The mathematical theory of equilibrium cracks in brittle fracture. *Advances in Applied Mechanics*, vol. VII, pp.55-129. Academic Press.

Brebbia, C. A., Telles, J. C. F., & Wrobel, L. C. , 1984. *Boundary Element Techniques: Theory and Applications in Engineering*. Prentice Hall, Berlin.

Crouch, S. L., & Starfield, A. M, 1983. *Boundary Element Methods in Solid Mechanics*. George Allen & Unwin, London.

Dumont, N. A., 1989. The hybrid boundary element method: an alliance between mechanical consistency and simplicity. *Applied Mechanics Reviews*, vol. 42, n. 11, part 2, pp. S54-S63.

Dumont, N. A., 2008. *Dislocation-Based Hybrid Boundary Element Method*. Draft paper.

Dumont, N. A., 2016. Fundamentals of the hybrid boundary element method. *To be submitted*.

Dumont, N. A., & Aguilar, C. A., 2012. The best of two worlds: The expedite boundary element method. *Engineering Structures*, vol. 43, pp. 235-244.

Dumont, N. A., Huaman, D., 2009. Hybrid finite/boundary element formulation for strain gradient elasticity problems. In Sapountzakis, E. J. & Aliabadi, M. H., eds., *Advances in Boundary Element Techniques X, Proceedings of the 10th International Conference*, pp. 295-300, EC, Ltd., UK.

Dumont, N. A., & Lopes, A. A. O., 2003. On the explicit evaluation of stress intensity factors in the hybrid boundary element method. *Fatigue & Fracture of Engineering Materials & Structures*, vol. 26, pp. 151-165.

Dumont, N. A., & Mamani, E. Y., 2011a. Use of generalized Westergaard stress functions as fundamental solutions. In Albuquerque, E. L. & Aliabadi, M. H., eds, *Advances in Boundary element Techniques XII*, pp 170-175, EC, Ltd., UK.

Dumont, N. A., & Mamani, E. Y., 2011b. Generalized Westergaard stress functions as fundamental solutions. *Computer Modeling in Engineering & Sciences*, vol. 78, n. 2, pp. 109-150.

Dumont, N. A. & Mamani, E. Y., 2013. Simulation of plastic zone propagation around crack tips using the hybrid boundary element method. In Del Prado, Z. J. G. N., ed, *CILAMCE – XXXIV Iberian Latin-American Congress on Computational Methods in Engineering*, 20 pp on CD, Pirenpolis, Brasil.

Irwin, G. R., 1957. Analysis of stresses and strain near the end of a crack traversing a plate. *Journal of Applied Mechanics*, vol. 24, pp. 361-364.

Lopes, A. A. O., 1998. *The Hybrid Boundary Element Method Applied to Fracture Mechanics Problems (in Portuguese)*. MSc. thesis, Pontifical Catholic University of Rio de Janeiro/Brazil.

Lopes, A. A. O., 2002. *Evaluation of Stress Intensity Factors with the Hybrid Boundary Element Method (in Portuguese)*. PhD. thesis, Pontifical Catholic University of Rio de Janeiro/Brazil.

Mamani, E. Y., 2011. *The Hybrid Boundary Element Method Based on Generalized Westergaard Stress Functions (in Portuguese)*. MSc. thesis, Pontifical Catholic University of Rio de Janeiro/Brazil.

Mamani, E. Y., 2015. *Crack modeling using generalized Westergaard stress functions in the hybrid boundary element method (in Portuguese)*. Ph.D. thesis, Pontifical Catholic University of Rio de Janeiro/Brazil.

Sneddon, I. N., 1946. The distribution of stress in the neighborhood of a crack in an elastic solid. *Proceedings of the Royal Society of London A*, vol. 187, pp. 229-260.

Tada, H., Ernst, H., & Paris, P., 1993. Westergaard stress functions for displacement-prescribed crack problems - I. *International Journal of Fracture*, vol. 61, pp. 39-53.

Tada, H., Ernst, H., & Paris, P., 1994. Westergaard stress functions for displacement-prescribed crack problems - II. *International Journal of Fracture*, vol. 67, pp. 151-167.

Telles, J. C. F., Castor, G. S. & Guimares, S., 1995. A numerical Green's function approach for boundary elements applied to fracture mechanics. *International Journal for Numerical Methods in Engineering*, vol. 38, pp. 3259-3274.

Westergaard, H. M., 1939. Bearing pressures and cracks. *Journal of Applied Mechanics*, vol. 6, pp. 49-53.

Williams, M. L., 1957. On the stress distribution at the base of a stationary crack. *Journal of Applied Mechanics*, vol. 24, pp. 109-114.